



**CU(II) COMPLEXES OF DERIVATIVES OF (THIOPHEN-2-YL)METHANAMINE:
DESIGN, SYNTHESIS, SPECTRAL CHARACTERIZATION, DNA BINDING
INVESTIGATIONS AND ANTIMICROBIAL ACTIVITY**

S. Udaya Laxmi ^a, N Nageswara Rao ^a, P. Ettaiah ^{a*}

^a Department of Chemistry, University college of Science, Osmania University, Hyderabad, Telangana. Email Id: udayasalluri2@gmail.com

Abstract: The synthesis and characterization of six new Schiff base ligands, including the imine ligands TMMCFP, TMMFMOP, TMMFP, TMMDMOP, TMMBD, and TMMDEP, as well as their complexes with 3D series copper metal, included elemental analyses, ¹H, ¹³C NMR, IR, ESI mass, UV-Visible, ESR, magnetic moment, and TGA investigations. A square planar shape is ascribed to the Cu (II) compounds based on the findings from the studies to surround the metal ion. Using UV-visible electronic, fluorescence, and viscosity studies, the interaction of synthesized metal complexes with calf thymus Deoxyribonucleic acid (CT-DNA) was investigated. The results of the study suggested that all of the metal complexes intercalated significantly with CT-DNA. By using gel electrophoresis to study DNA cleavage studies with metal (II) complexes and highly coiled P^{BR322} DNA in the presence of Hydrogen peroxide (H₂O₂) and UV light, it was discovered that the aforementioned Cu(II) compounds cut DNA more efficiently. All of the complexes of metals are shown to be more powerful than free ligands when it comes to the antibacterial activity of both the ligands and their corresponding metal compounds.

Keywords: Ligands; Cu(II) Complexes; DNA interactions; Photo cleavage; antibacterial activity.

1. Introduction

The growth of coordination chemistry has largely been facilitated by Schiff base ligands. It is common knowledge that a variety of metal ions may combine with ligands having nitrogen and oxygen (N₂O₂) donor atoms in the azomethine base. They have generated a lot of attention recently because of how simple they are to synthesize, how stable they are under different oxidizing and reducing circumstances, and how flexible their design is in terms of all of the uses they may be used for [i-iii]. Because of its biocide properties against bacteria, fungus, and specific types of drugs, 3D series metals Schiff base complexes have a wide variety of uses [iv, v]. Certain medications have enhanced efficacy when given as metal chelates and prevent the formation of tumors [xi, vii]. Furthermore, as several of these complexes have been shown to be

potential models for physiologically significant species, the discipline of bioinorganic chemistry has developed, which has raised interest in Schiff base complexes [viii-x]. Because of their strong nonlinear responses, those substances are also used in optoelectronic and magnetic technologies [xi-xiii]. It is evident that the low cost, ease of preparation, and chemical and thermal stability of Schiff base 3D series I-B metal complexes make them essential chelates. Schiff bases are often ligands that may form extremely stable compounds with transition metals, such as bidentate [xiv, xv], tridentate, tetra dentate, and polydentate [xvi, xvii]. Only when they have a functional group typically the hydroxyl near enough to the condensation site to allow for the formation of a 5 or 6 membered ring upon reaction with a metal ion can they function as coordinating ligands. Additionally, N and O donor atoms are crucial to the processes of change of certain reactions in unaffected biological systems, particularly when functional groups like -OH is present close to the azomethine (-HC=N) group and forms a five- or six-membered ring with the metal ion [xviii]. In addition to offering a platform for amazing biological activity, the imine (-C=N-) group of Schiff base ligands has several uses in the food and dye industries, agrochemicals, analytical chemistry, and catalysis [xix, xx]. Many studies have been conducted on transition metal complexes with Schiff base ligands as antibacterial and anticancer agents.

2. MATERIALS

2.1 Required chemicals, solvents and bio chemicals

5-(Thiophen-2-yl)methoxybenzenamine, 3,5-dichlorosalicylaldehyde, 3-methoxy-5-bromo salicylaldehyde, 3-bromo-5-chlorosalicylaldehyde, 4-methoxysalicylaldehyde, 4,6-dimethoxy salicylaldehyde, 4-hydroxysalicylaldehyde and 4-methyl salicylaldehydes obtained from BLD company and solvents methyl alcohol, EtOAC, MDC, dimethyl sulphoxide (DMSO), hydrochloric acid (HCl), acetone, Chloroform (CHCl₃), acetonitrile (CH₃CN), sulphuric acid and copper(II) acetate monohydrate procured from avra company analytical grade. The Ethidium bromide, EDTA, Tris buffer and Glacial acetic acid were obtained from Merck (India). Calf thymus DNA (CT-DNA) were purchased from Genei, Bangalore and stored at 0-5 °C.

3. Physical measurements

During the course of this study, all synthesized compounds were characterized using a variety of techniques, including Infrared, Mass, NMR (¹H and ¹³C-NMR), elemental analysis, Melting point and electronic absorption spectral techniques. A brief discussion is given of these physical procedures. Using potassium bromide pellets, FT-IR spectrophotometers (Shimadzu 8400S) captured IR spectra in the 250–4000 cm⁻¹ range. All of the compounds' ESI mass spectra have been acquired using the VG AUTOSPEC mass spectrometer. With TMS serving as the internal standard, the ligands ¹H and ¹³C-NMR spectra were obtained on a Bruker 400 MHz NMR device.

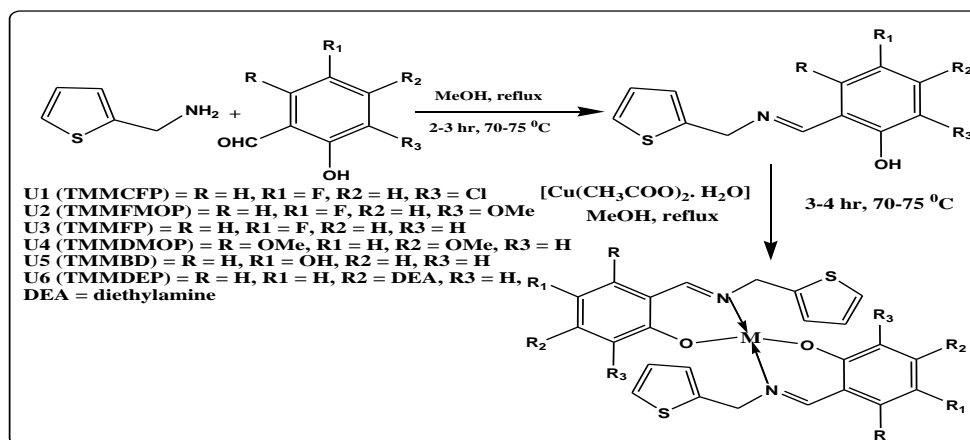
The Elementary Vario EL III micro analyser was utilised to determine the elemental analysis by micro analytical procedures. The complex's uncorrected melting point (M.P.) was determined using open glass capillary Galen Kamp equipment. A Shimadzu UV-Vis 2600 was used to record the compounds' UV-Visible spectra. Using Hg [Co(NCS)₄] as a reference, the magnetic moments of the copper(II) compounds have been determined on the Gouy balance model 7550. Using DPPH as an internal standard, the X-band ESR spectra of Cu(II) complexes in DMSO were recorded on a Varian ESR spectrometer at both ambient temperature (300 K) and liquid nitrogen environments (77). The Shimadzu TGA-50H thermal analyses was used to perform thermo gravimetric analysis of complexes in an evolving nitrogen environment (20 mL min⁻¹) at temperatures ranging from room temperature to 1200 °C, employing a rate of heating of 10 °C

min⁻¹. With a xenon lamp and a 1 cm-long rectangular quartz cuvette at 25 °C, the JASCO spectrofluorometric FP-8500 was used for measuring the fluorescence emission spectra.

4. Synthesis of U1-U6 N-O donor ligands and Metal complexes

4.1 General Synthesis of U1-U6 N-O donor ligands

The 1mmol of hot carbinol solution of 6-Aminobenzothiazole was added slowly drop-wise to the respective 1mmol of hot carbinol solutions of various aromatic aldehydes. 3,5-dichlorosalicylaldehyde, 3-methoxy-5-bromosalicylaldehyde, 3-bromo-5-chlorosalicylaldehyde, 4-methoxysalicylaldehyde, 4,6-dimethoxysalicylaldehyde, 4-hydroxysalicylaldehyde, and 4-methylsalicylaldehyde in a **1:1** equimolar ratio. The ensuing combination was refluxed for two to four hours, and the solid product that was produced was filtered, vacuum-dried, and recrystallized from hot carbinol. (**Scheme –SI**)



Scheme –SI: Synthesis of U1-U6 N-O donor ligands and metal complexes

4.2. Synthesis of M1-M6 metal complexes

M1-M6 mono nuclear 3d series transition metal complexes are produced by adding the hot methyl alcohol solution of IB group Cu(II) acetate mono hydrate into a stirred hot methyl alcohol solution of the various imine ligands TMMCFP, TMMFMOP, TMMFOP, TMMDMOP, TMMBD, and TMMDEP in One : Two molar ratio (1:2). Temperature was maintained at 70–75 °C while the reaction mixture was refluxed over an oil bath for 3-4 hrs. After being separated and filtered, the solid product washed away using Carbinol and petroleum ether. (**Scheme –SI**)

4.3. Characterization of U1-U6 N-O donor ligands

4.3.1. U1 Ligand (TMMCFP)

Analytical data: IR (KBr/Cm⁻¹): 3451 (OH); 1628 (CH=N); 1273 (C-O), 829 (C-S-C) (**Fig-UL1**). Mass: 271 [M+H]⁺. Proton NMR: 400 MHz, CDCl₃, δ: 12.06 (s, 1H, OH), 9.27 (s, 1H, azomethine-H), 7.51-7.01 (m, 5 ArH, s), 4.51 (s, 2H, -CH₂-N=) (**Fig-UL3**). Carbon NMR: 100 MHz, CDCl₃, (δ):195.3, 166.6, 160.9, 139.6, 135.9, 135.6, 121.7, 119.7, 111.3, 104.1, 103.9, and 41.1. Elemental analysis: M.F: C₁₂H₉ClFNOS, Found: C, 53.51; H, 3.41; N, 5.23; S, 11.94. Calculated: C, 53.44; H, 3.36; N, 5.19; S, 11.89. M.P: 135°C. UV-Vis (λ_{max}): 280 and 344 nm (**Fig-UL2**). Yield: 78%.

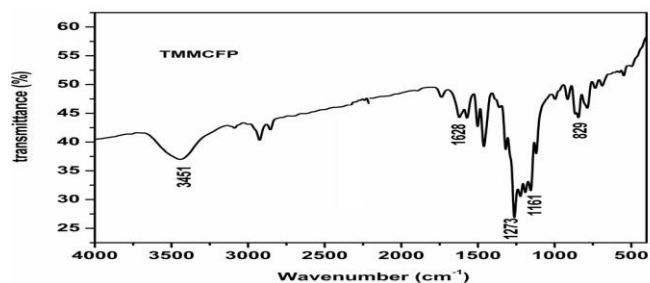


Fig-UL1. IR spectra of TMMCFP

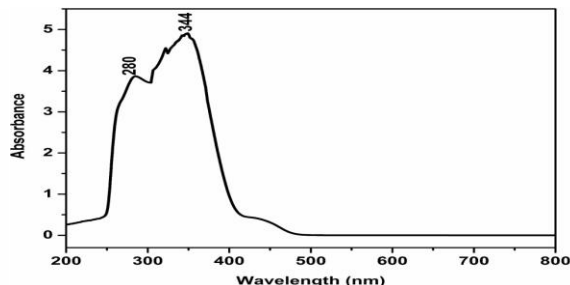


Fig-UL2. Uv-Vis spectra of TMMCFP

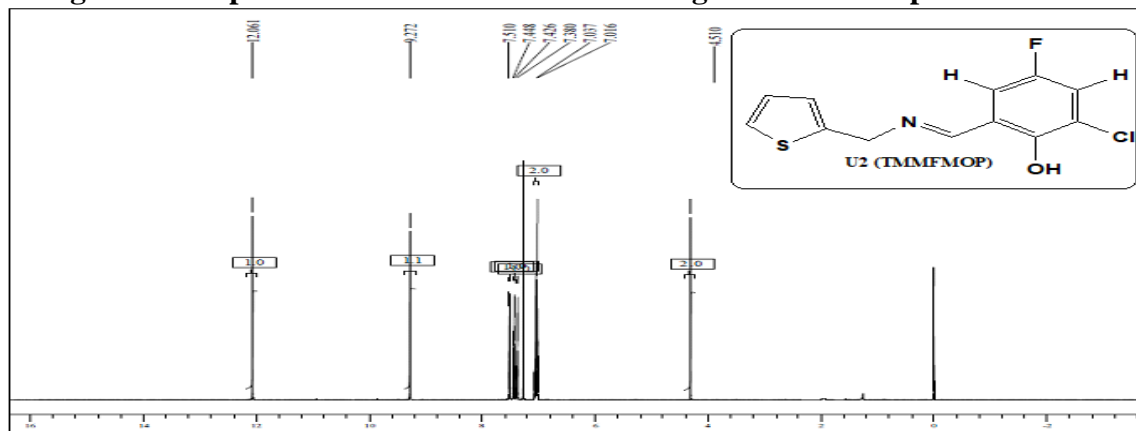


Fig-UL3. ¹H NMR spectra of TMMCFP

4.3.2. U2 Ligand (TMMFMOP)

Analytical data: IR (KBr/ cm^{-1}): 3462 (OH); 1620 (CH=N); 1247 (C-O), 853 (C-S-C) (**Fig-UL4**). Mass: 265 [M]. Proton NMR: 400 MHz, CDCl_3 , δ : 13.12 (s, 1H, OH), 8.34 (s, 1H, azomethine-H), 7.23-6.69 (m, 5 ArH, s), 4.91 (s, 2H, -CH₂-N=), 3.32 (s, 3H, -OCH₃) (**Fig-UL6**). Carbon NMR: 100 MHz, CDCl_3 , (δ): 165.4, 161.0, 143.5, 141.0, 131.4, 127.0, 125.3, 125.0, 119.8, 117.4, 116.4, 57.3, and 41.8. Elemental analysis: M.F: C₁₃H₁₂FNO₂S, Found: C, 58.90; H, 5.60; N, 5.34; S, 12.13. Calculated: C, 58.85; H, 4.56; N, 5.28; S, 12.09. M.P: 161 °C. UV-Vis (λ_{max}): 277 and 391 nm (**Fig-UL5**). Yield: 73%.

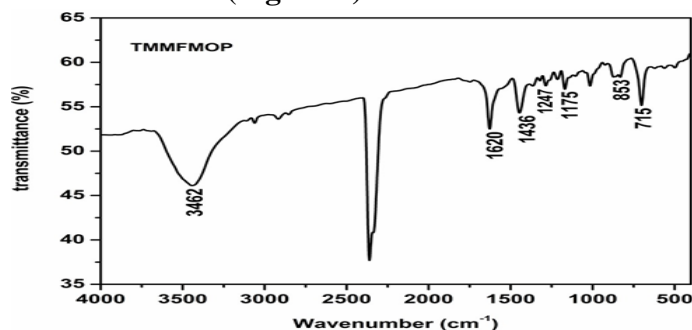


Fig-UL4. IR spectra of TMMFMOP

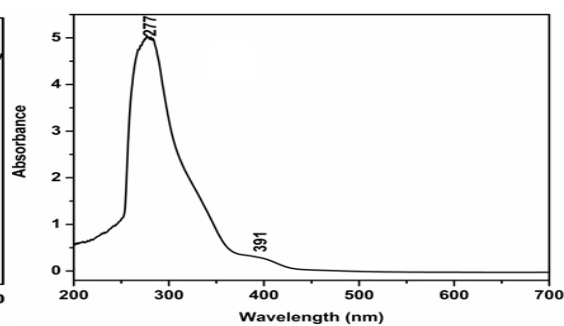


Fig-UL5. Uv-Vis spectra of TMMFMOP

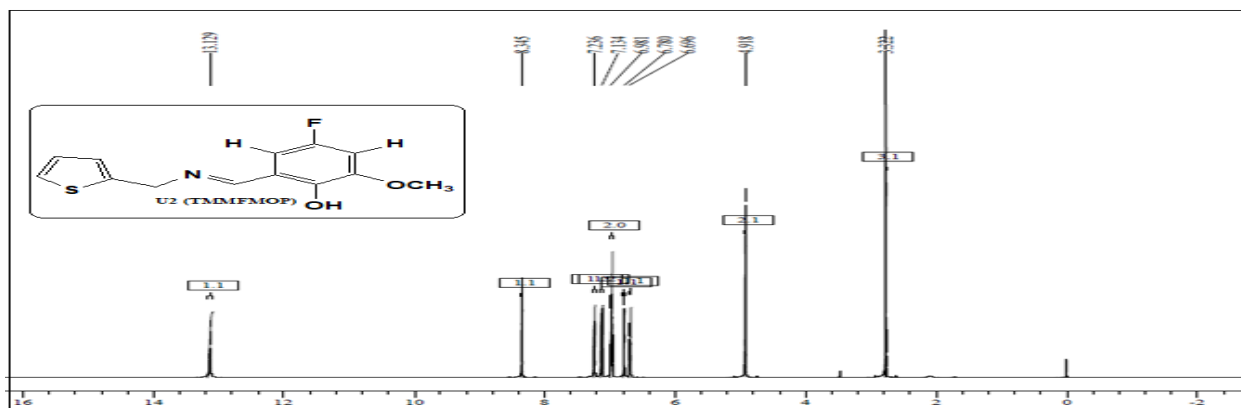


Fig-UL6. ¹H NMR spectra of TMMFMOP

4.3.3. U3 Ligand (TMMFP)

Analytical data: IR (KBr/Cm⁻¹): 3449 (OH); 1616 (CH=N); 1228 (C-O), 824 (C-S-C) (Fig-UL7). Mass: 236 [M+H]⁺. Proton NMR: 400 MHz, CDCl₃, δ: 14.23 (s, 1H, OH), 8.26 (s, 1H, azomethine-H), 7.56-7.00 (m, 6ArH, s), 5.00 (s, 2H, -CH₂-N=) (Fig-UL9). Carbon NMR: 100 MHz, CDCl₃, (δ): 163.7, 157.2, 138.9, 135.2, 129.9, 127.2, 126.2, 125.7, 123.2, 119.3, 111.8, and 56.3. Elemental analysis: M.F: C₁₂H₁₀FNOS, Found: C, 61.30; H, 4.31; N, 6.00; S, 13.66. Calculated: C, 61.26; H, 4.28; N, 5.95; S, 13.63. M.P: 145°C. UV-Vis (λ_{max}): 263 and 393 nm (Fig-UL8). Yield: 70%.

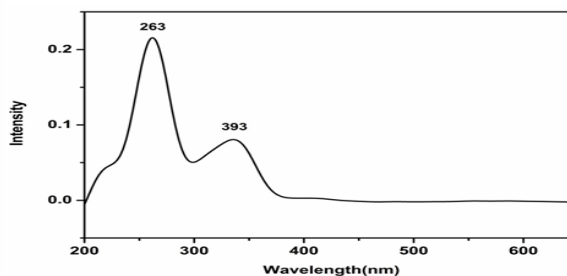
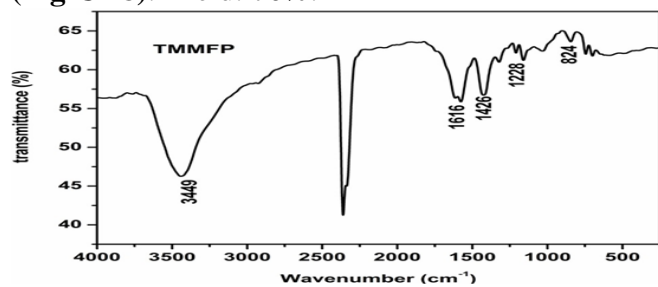


Fig-UL7. IR spectra of TMMFP

Fig-UL8. Uv-Vis spectra of TMMFP

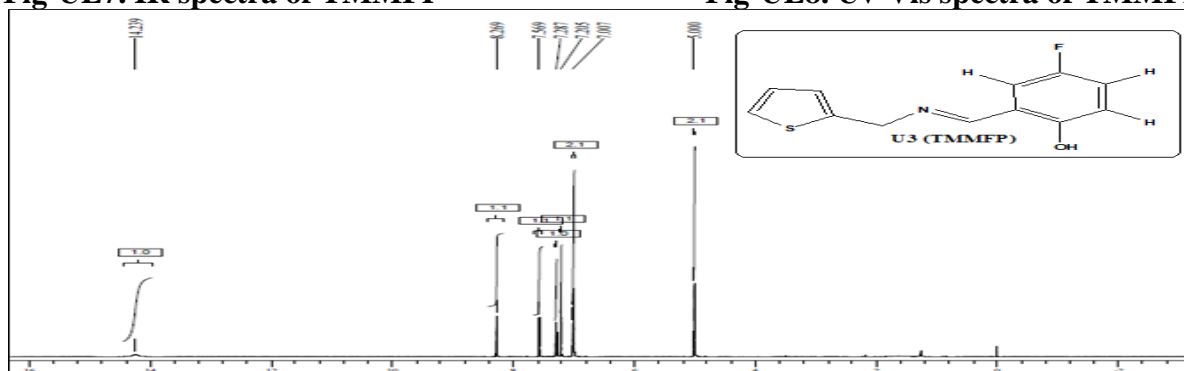


Fig-UL9. ¹H NMR spectra of TMMFP

4.3.4. U4 Ligand (TMMDMOP)

Analytical data: IR (KBr/Cm⁻¹): 3454 (OH); 1631 (CH=N); 1206 (C-O), 825 (C-S-C) (Fig-UL10). Mass: 277 [M]. Proton NMR: 400 MHz, CDCl₃, δ: 14.56 (s, 1H, OH), 8.90 (s, 1H, azomethine-H), 7.25-5.9 (m, 5ArH, s), 5.08 (s, 2H, -CH₂-N=), 3.82 (s, 6H, -OCH₃) (Fig-UL12). Carbon NMR: 100 MHz, CDCl₃, (δ): 167.0, 165.8, 161.1, 157.5, 147.0, 146.6, 122.0, 121.7, 103.3, 93.7, 92.9, 90.0, 55.7, and 45.6. Elemental analysis: M.F: C₁₄H₁₅NO₃S, Found: C, 30.69;

H, 5.51; N, 5.11; S, 11.62. Calculated: C, 60.63; H, 5.45; N, 5.05; S, 11.56. M.P: 153 °C. UV-Vis (λ_{\max}): 280 and 344 nm (**Fig-UL11**). Yield: 75%.

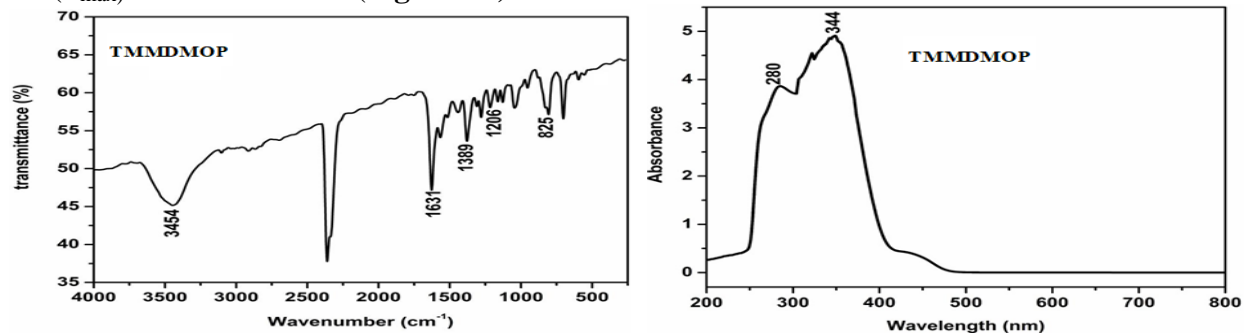


Fig-UL10. IR spectra of TMMDMOP

Fig-UL11. Uv-Vis spectra of TMMDMOP

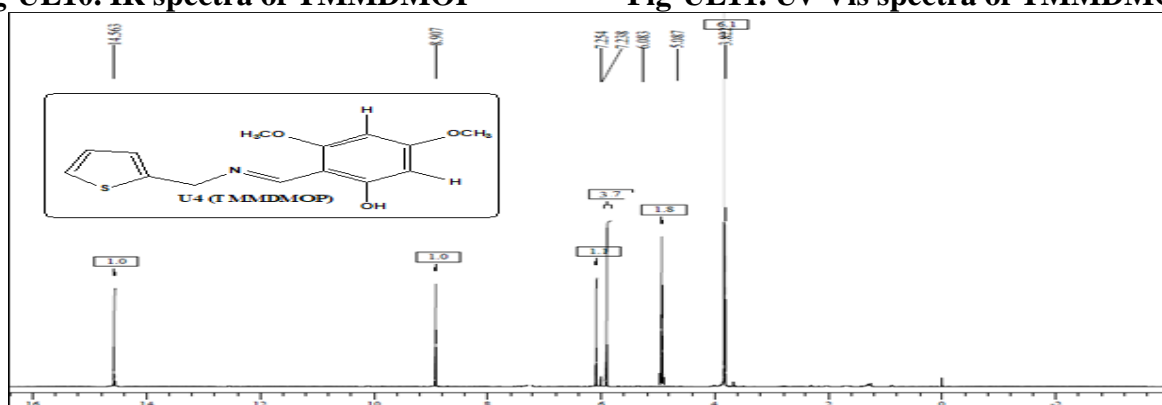


Fig-UL12. ¹H NMR spectra of TMMDMOP

4.3.5. U5 Ligand (TMMBD):

Analytical data: IR (KBr/Cm⁻¹): 3461 (OH); 1625 (CH=N); 1201 (C-O), 826 (C-S-C) (**Fig-UL13**). Mass: 233 [M]. Proton NMR: 400 MHz, CDCl₃, δ : 12.60 (s, 2H, OH), 9.00 (s, 1H, azomethine-H), 8.62-6.91 (m, 6ArH, s), 5.00 (s, 2H, -CH₂-N=) (**Fig-UL15**). Carbon NMR: 100 MHz, CDCl₃, (δ): 168.0, 162.1, 135.8, 134.3, 119.9, 118.2, 117.7, 104.0, 103.8, 102.9, 102.7, 57.6. Elemental analysis: M.F: C₁₂H₁₁NO₂S, Found: C, 61.84; H, 4.81; N, 6.04; S, 13.81. Calculated: C, 61.78; H, 4.75; N, 6.00; S, 13.74. M.P: 142 °C. UV-Vis (λ_{\max}): 291 and 350 nm (**Fig-UL14**). Yield: 68%.

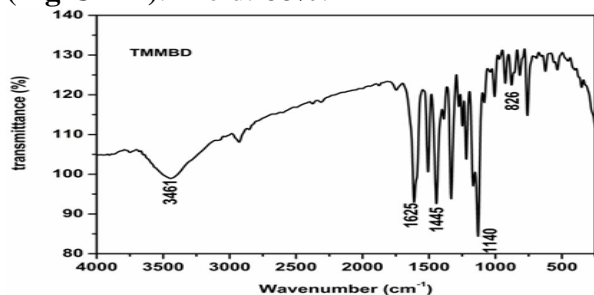


Fig-UL13. IR spectra of TMMBD

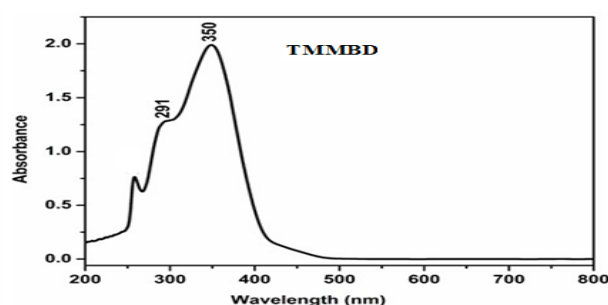


Fig-UL14. Uv-Vis spectra of TMMBD

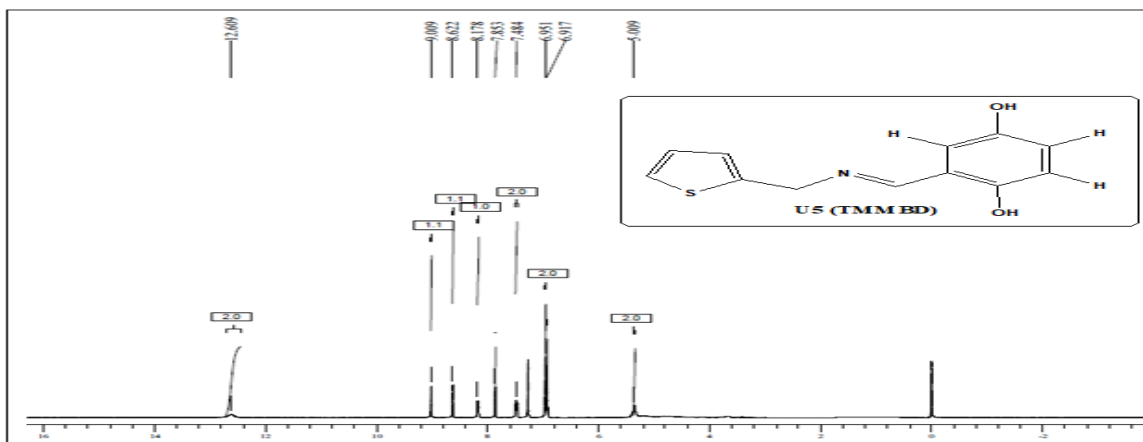


Fig-UL15. ¹H NMR spectra of TMMBD

4.3.6. U6 Ligand (TMMDEP):

Analytical data: IR (KBr/Cm⁻¹): 3443 (OH); 1623 (CH=N); 1167 (C-O), 863 (C-S-C) (**Fig-UL16**). Mass: 289 [M+H]⁺. Proton NMR: 400 MHz, CDCl₃, δ: 13.47 (s, 1H, OH), 11.64 (s, 1H, azomethine-H), 9.47-6.606 (m, 6 ArH, s), 4.14 (s, 2H, -CH₂-N=), 3.40 (s, 4H, -CH₂-), 1.20 (s, 6H, -CH₃) (**Fig-UL18**). Carbon NMR: 100 MHz, CDCl₃, (δ): 164.3, 163.8, 161.2, 152.0, 147.8, 146.6, 135.4, 133.9, 121.9, 104.3, 103.9, 97.6, 44.8, 44.6, 12.7, and 12.5. Elemental analysis: M.F: C₁₆H₂₀NO₂S, Found: C, 66.68; H, 7.04; N, 9.77; S, 11.18. Calculated: C, 66.63; H, 6.99; N, 9.71; S, 11.12. M.P: 163 °C. UV-Vis (λ_{max}): 262 and 415 nm (**Fig-UL17**). Yield: 60%.

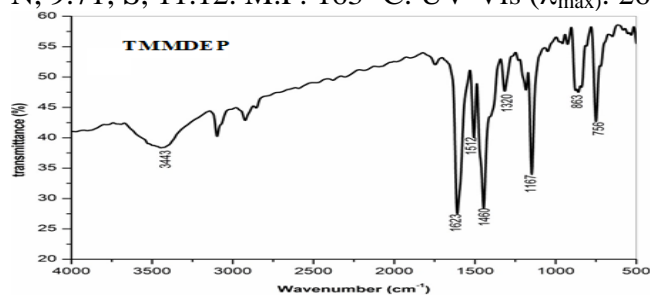


Fig-UL16. IR spectra of TMMDEP

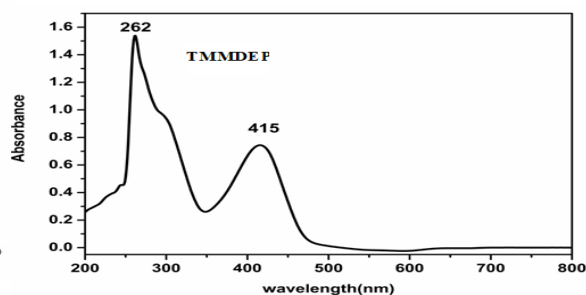


Fig-UL17. Uv-Vis spectra of TMMDEP

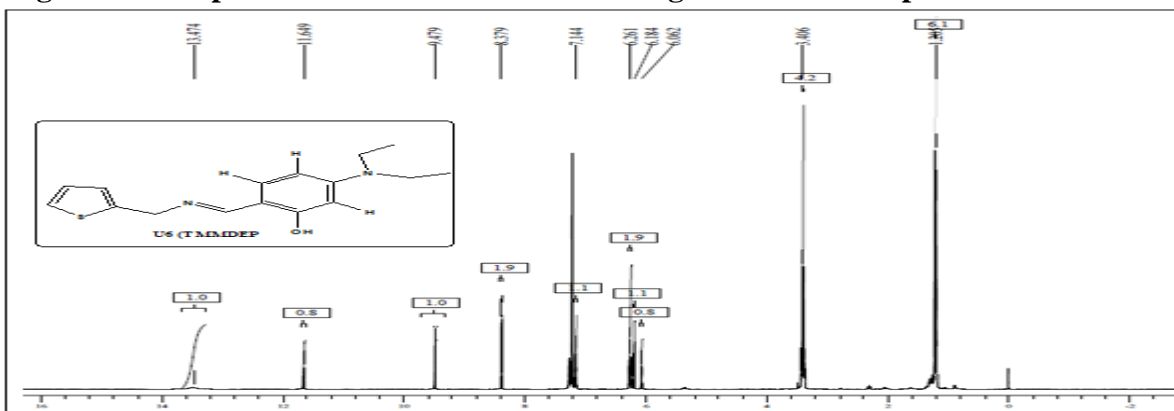


Fig-UL18. ¹H NMR spectra of TMMDEP

4.4 Characterizations of M1-M6 metal complexes

4.4.1. [Cu(TMMCFP)₂] (M1)

Analytical data: Mass: [M+H]⁺ 602; M.P: 312-314 °C; IR (ν): 1612 (CH=N), 1238 (C–O), 829 (C–S–C), 589 (M–O), 429 (M–N). Elemental analysis: C₂₄H₁₆Cl₂CuF₂N₂O₂S₂: calculated (found): C; 47.96 (47.96), H; 2.68 (2.72), N; 4.66 (4.71), Cu; 10.57 (10.63). UV-Vis: 257, 381, 561. ESR: g_{||}; 2.16, g_⊥: 2.04, G: 3.65. μ_{eff}(BM): 1.73. Yield: 59%

4.4.2. [Cu(TMMFMOP)₂] (M2)

Analytical data: Mass: [M+H]⁺ 592; M.P: 300-302 °C; IR (ν): 1635 (CH=N), 1262 (C–O), 853 (C–S–C), 559 (M–O), 462 (M–N). Elemental analysis: C₂₆H₂₂CuF₂N₂O₄S₂: calculated (found): C; 43.81 (43.974), H; 3.11 (3.19), N; 3.92 (3.97), Cu; 8.90 (8.96). UV-Vis: 259, 344, 480. ESR: g_{||}; 2.17, g_⊥: 2.05, G: 3.33. μ_{eff}(BM): 1.76. Yield: 62%.

4.4.3. [Cu(TMMFP)₂] (M3)

Analytical data: Mass: [M+H]⁺ 532; M.P: 330-332 °C; IR (ν): 1607 (CH=N), 1152 (C–O), 824 (C–S–C), 502 (M–O), 449 (M–N). Elemental analysis: C₂₄H₁₈CuF₂N₂O₂S₂: calculated (found): C; 54.17 (54.23), H; 3.41 (3.46), N; 5.26 (5.30), Cu; 11.94 (11.98). UV-Vis: 310, 392, 525. ESR: g_{||}; 2.07, g_⊥: 2.02, G: 3.82. μ_{eff}(BM): 1.81. Yield: 60%

4.4.4. [Cu(TMMDMOP)₂] (M4)

Analytical data: Mass: [M+H]⁺ 616; M.P: 318-320 °C; IR (ν): 1612 (CH=N), 1121 (C–O), 825 (C–S–C), 589 (M–O), 520 (M–N). Elemental analysis: C₂₈H₂₈CuN₂O₆S₂: calculated (found): C; 54.58 (54.62), H; 4.58 (5.03), N; 4.63 (4.55), Cu; 10.31 (10.37). UV-Vis: 256, 432, 526, 557. ESR: g_{||}; 2.17, g_⊥: 2.11, G: 1.22. μ_{eff}(BM): 1.78. Yield: 55%.

4.4.5. [Cu(TMMBD)₂] (M5)

Analytical data: Mass: [M+H]⁺ 528; M.P: 338-340 °C; IR (ν): 1614 (CH=N), 1115 (C–O), 826 (C–S–C), 604 (M–O), 482 (M–N). Elemental analysis: C₂₄H₂₀CuN₂O₄S₂: calculated (found): C; 54.58 (54.62), H; 3.82 (3.85), N; 5.30 (5.35), Cu; 12.03 (12.08). UV-Vis: 265, 414, 555. ESR: g_{||}; 2.13, g_⊥: 2.04, G: 3.38. μ_{eff}(BM): 1.79. Yield: 58%.

4.4.6. Cu(TMMDEP)₂] (M6)

Analytical data: Mass: [M+H]⁺ 638; M.P: >321 °C; IR (ν): 1614 (CH=N), 1151 (C–O), 864 (C–S–C), 505 (M–O), 408 (M–N). Elemental analysis: C₃₂H₃₈CuN₄O₂S₂: calculated (found): C; 60.21 (60.25), H; 6.00 (6.07), N; 8.78 (8.82), Cu; 9.95 (10.01). UV-Vis: 260, 336, 428, 571. ESR: g_{||}; 2.24, g_⊥: 2.05, G: 4.19. μ_{eff}(BM): 1.74. Yield: 62%.

5. DNA Investigations

5.1. UV-Vis Absorption spectra

In this study, an absorption titration experiment was conducted using a fixed amount of the Cu(II) complex. The synthesized compound was dissolved in a solvent mixture consisting of 1% DMSO and 99% Tris-HCl buffer (5 mM Tris-HCl; 50 mM NaCl, pH 7.1) for subsequent absorption titration experiments. Absorption titration experiments were carried out both in the absence and presence of varying concentrations of CT DNA. During the measurement of absorption spectra, CT-DNA was introduced to the compound solution as well as the reference solution to eliminate the absorbance contribution from CT-DNA itself. The absorption titration data were analyzed to determine the binding constant (K_b) using the following **equation. 1 [xxi-xxiii]**

$$[\text{DNA}] / (\epsilon_a - \epsilon_f) = [\text{DNA}] / (\epsilon_b - \epsilon_f) + 1 / K_b [(\epsilon_b - \epsilon_f)] \quad (1)$$

In the context of the experiment, [DNA] represents the concentration of DNA, while ϵ_a , ϵ_f , and ϵ_b represents the apparent absorption coefficient, the extinction coefficient of the compounds without DNA, and the extinction coefficient of the compound with DNA, respectively, K_b binding constant

5.2. Study of Fluorescence

Employing a fluorescence spectrophotometer, the study focused on investigating the interactions between metal complexes and DNA. In a pH 7.2 Tris-HCl/NaCl buffer, Deoxyribonucleic acid (DNA) was pre-treated with ethidium bromide (EB) at a fixed ratio of [CT-DNA]/[EB] = 10 for a duration of 30 minutes. The Stern-Volmer equation (**Equation 2**) was utilized to calculate the binding interactions of the complexes. [xxiv, xxv]

$$\frac{I_0}{I} = 1 + K_{sv} r \quad (2)$$

In the absence (I_0) or presence (I) of the complexes, the fluorescence intensity was designated, The linear Stern-Volmer value, denoted as K_{sv} , and the complex concentration in DNA proportions, represented by r .

5.3. Study of Antibacterial activities

Petri plates were inoculated with actively growing cultures of the bacterial strains. The prepared discs were placed on antibiotic nutrient agar broth in Petri plates, seeded with 1 mL of bacterial culture, and incubated for 24 hours at 37°C. After 24 hours, the Petri dishes were examined for the presence of a growth inhibition zone. A clear zone of growth inhibition around the paper disc indicated the antibacterial activity of the compound. The diameter of the zone of inhibition was measured in millimetres as an indicator of the compound's efficacy. Streptomycin was utilized as a standard drug for comparative analysis. The observed results were compared to the standard drug, streptomycin, to assess the relative antibacterial activity. [xxvi-xxviii]

5.4. Antifungal activity

The well diffusion method was employed to assess the anti-fungal activity of chemical compounds, with concentrations of the test compounds at various concentrations. Potato Dextrose agar culture plates were prepared and subjected to *M. phaseolina* and *S. rolfsii* fungi using the spread plate method. Incubation occurred at 37±2 °C for 48 hours to gauge fungal activity. Following incubation, zones around the wells were inspected, and the zone of inhibition (mm) was measured. The activity index was calculated, and readings were collected in three fixed directions within three replicates. Average values were tabulated for comprehensive interpretation. [xix-xxxi]

6. Results and Discussion

6.1. FT-IR Spectra

The IR spectra analysis of the Schiff base ligands, namely TMMCFP (**U1**), TMMFMOP (**U2**), TMMFP (**U3**), TMMDMOP (**U4**), TMMBD (**U5**), and TMMDEP (**U6**), and their corresponding 3d series Cu(II) complexes [Cu(TMMCFP)₂] (**M1**), [Cu(TMMFMOP)₂] (**M2**), [Cu(TMMFP)₂] (**M3**), [Cu(TMMDMOP)₂] (**M4**), [Cu(TMMBD)₂] (**M5**), and [Cu(TMMDEP)₂] (**M6**), is presented in **Table-T1**. The major peaks and spectra for each compound are illustrated in **Fig-UL19-UL25**. To investigate the binding mode of the Schiff base ligands to the metal ions in the complexes, the IR spectrum of each free Schiff base ligand was compared with the spectra of its corresponding complex. The IR spectra of the Schiff bases exhibit a broad band in the range of 3443–3462 cm⁻¹, assigned to the (OH) group. The absence of this band in the complex spectra suggests the deprotonating of the hydroxyl group and coordination through the deprotonated phenolic OH group. A strong intense band observed at 1201-1273 cm⁻¹ in the Schiff bases,

attributed to phenolic C–O stretching, undergoes a shift in the metal complexes, indicating coordination through the phenolic oxygen to the metal atom. Additionally, the Schiff base ligands show a robust band in the region of 1167-1273 cm^{-1} corresponding to the azomethine (C=N) group. This band experiences a shift in the metal complexes, signifying coordination of the imine group nitrogen to the M(II) ion. In the free Schiff base ligands, a sharp band at 823-853 cm^{-1} is observed, attributed to the (–C–S–C) stretching frequency of the thiophene ring. This band remains relatively unchanged in all complexes, confirming the non-involvement of the thiophene sulfur in complex formation. Furthermore, the coordination of the azomethine nitrogen and phenolic oxygen is supported by the appearance of two bands at 504-604 cm^{-1} and 408-520 cm^{-1} , corresponding to $\nu\text{M–O}$ and $\nu\text{M–N}$, respectively. [xxxii-xxxiv]

Table-T1: The vibrational frequencies observed in the IR spectra reflect the structural characteristics of the Schiff bases and their respective metal complexes.

Compound	$\nu(\text{OH})$	$\nu(\text{C=N})$	$\nu(\text{C-O})$	$\nu(\text{C-S-C})$	$\nu(\text{M-O})$	$\nu(\text{M-N})$
TMMCFP	3451	1628	1273	829	-	-
[Cu(TMMCFP) ₂]	-	1612	1238	829	589	429
TMMFMOP	3462	1620	1247	853	-	-
[Cu(TMMFMOP) ₂]	-	1635	1262	853	559	462
TMMFP	3449	1616	1228	824	-	-
[Cu(TMMFP) ₂]	-	1607	1152	824	502	449
TMMDMOP	3454	1631	1206	825	-	-
[Cu(TMMDMOP) ₂]	-	1612	1121	825	589	520
TMMBD	3461	1625	1201	826	-	-
[Cu(TMMBD) ₂]	3448	1614	1115	826	604	482
TMMDEP	3443	1623	1167	863	-	-
[Cu(TMMDEP) ₂]	-	1614	1151	864	505	408

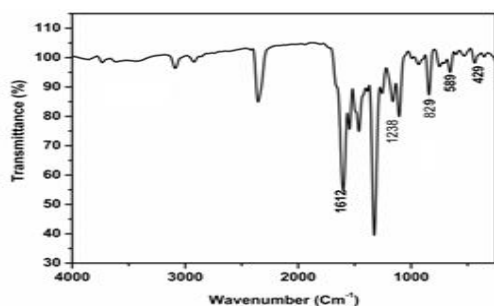


Fig-UL19. IR of [Cu(TMMCFP)₂]

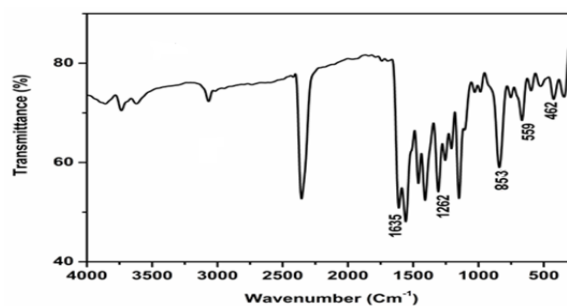


Fig-UL20. IR of [Cu(TMMFMOP)₂]

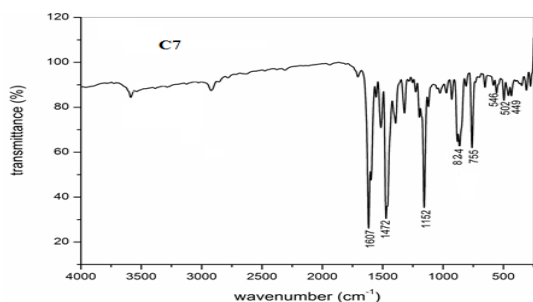


Fig-UL21. IR of [Cu(TMMFP)₂]

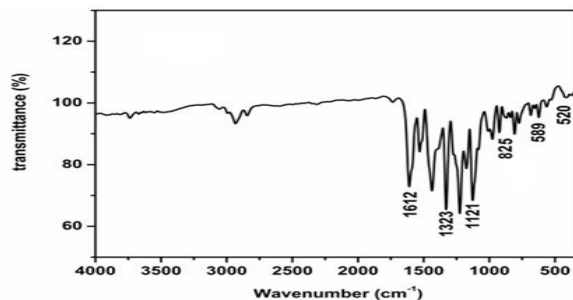


Fig-UL23. IR of [Cu(TMMDMOP)₂]

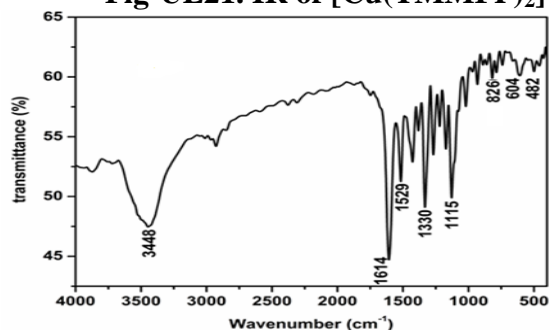


Fig-UL24. IR of [Cu(TMMBD)₂]

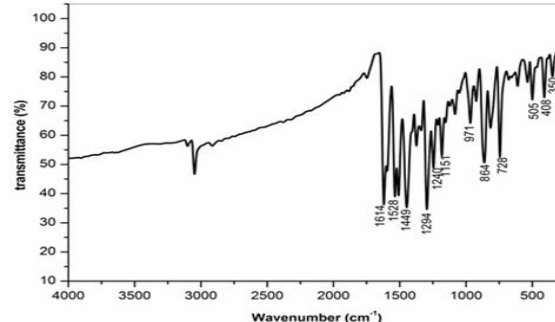


Fig-UL25. IR of [Cu(TMMDEP)₂]

6.2 Mass spectral analysis

The metal complexes (M1-M6) were subjected to detailed characterization through electrospray ionization mass spectrometry (ESI-MS), allowing for the identification of the active chemical species in solution and this information is meticulously documented in **Table-T2**. [xxxv, xxxvi] **Table-T2**. Provides the electrospray ionization mass spectrometry (ESI-MS) data for the Cu(II) complexes represents as **M1-M6**

Complex	Obtained	calculated
[Cu(TMMCFP) ₂] (M1)	602 [M+2H] ⁺	600
[Cu(TMMFMOP) ₂] (M2)	592 [M+H] ⁺	591
[Cu(TMMFP) ₂] (M3)	532 [M+H] ⁺	531
[Cu(TMMDMOP) ₂] (M4)	616 [M+H] ⁺	615
[Cu(TMMBD) ₂] (M5)	528 [M+H] ⁺	527
[Cu(TMMDEP) ₂] (M6)	638 [M+H] ⁺	637

6.3. ESR spectral studies

To validate the structural geometry of the Cu(II) complexes [Cu(TMMCFP)₂], [Cu(TMMFMOP)₂], [Cu(TMMFP)₂], [Cu(TMMDMOP)₂], [Cu(TMMBD)₂] and [Cu(TMMDEP)₂], through electronic paramagnetic resonance (EPR) spectroscopy was employed. EPR spectra of the Cu(II) complexes were acquired in a frozen dimethyl sulfoxide (DMSO) solution at 77 K using X-band spectroscopy, as illustrated in **Fig-UL26**. **Table-T3**. Lists the spin Hamiltonian parameters obtained from the EPR spectra, providing essential information about the electronic and magnetic properties of the investigated Cu(II) complexes. The observed EPR spectra reveal an anisotropic signal characteristic of monomeric Cu(II) complexes. This feature arises from the d9 electron configuration of the Cu(II) center, interacting

with the nuclear spin ($I=3/2$). Notably, the g_{\parallel} and g_{\perp} values deviate from the expected g_e value (2.0023), indicating ligand bonding to copper. The observed order $g_{\parallel} > g_{\perp} > g_e$ is indicative of axial symmetry, suggesting a ground state with a square planar geometry around the Cu(II) center. The axial symmetry parameter 'G', determined by the Hathaway expression ($G = (g_{\parallel} - 2.0023)/(g_{\perp} - 2.0023)$), offers insights into the exchange interaction between copper centers. A G value less than 4 suggests considerable exchange interaction, while G values exceeding 4 indicate negligible exchange interaction. In summary, the EPR spectroscopy results provide a comprehensive understanding of the electronic and geometric characteristics of the investigated Cu(II) complexes, further confirming their structural features. [xxxvii-xxxix]

Table-T3. Displays the ESR data for Cu(II) complexes recorded at low temperatures (at 77 K)

Complex	g_{\parallel}	g_{\perp}	G
[Cu(TMMCFP) ₂] M1	2.16	2.04	3.65
[Cu(TMMFMOP) ₂] M2	2.17	2.05	3.33
[Cu(TMMFP) ₂] M3	2.07	2.02	3.82
[Cu(TMMDMOP) ₂] M4	2.17	2.11	1.22
[Cu(TMMBD) ₂] M5	2.13	2.04	3.38
[Cu(TMMDEP) ₂] M6	2.24	2.05	4.19

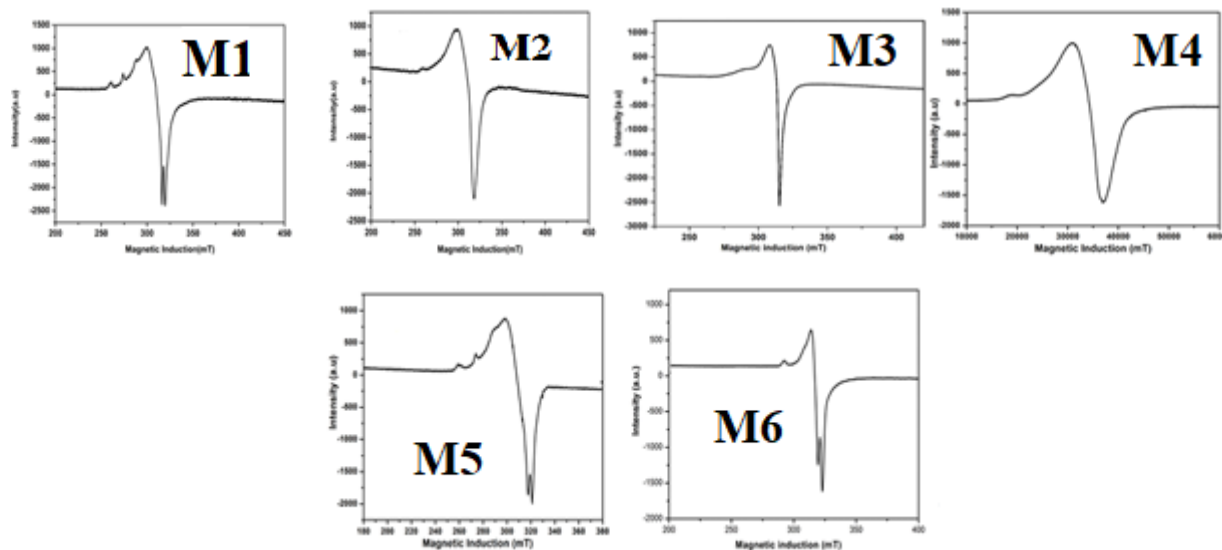


Fig-UL26 ESR spectrum of complex **M1-M6** metal complexes

6.4. Thermal analysis

TGA (Thermo gravimetric analysis) stands as a valuable technique employed to assess the thermal stability of Cu(II) complexes. The comprehensive thermal analysis of all Cu(II) complexes was conducted under a nitrogen atmosphere, employing a heating rate of 10 °C/min across a temperature range from ambient temperature to 1000 °C. The resulting thermo grams, illustrated in **Fig-UL27**, provide a visual representation of weight changes with increasing temperature. During TGA, the weight variation of a compound is tracked as temperature increases, and the resulting data is graphically represented in the form of a thermo gram, plotting weight against temperature. In the crystal lattices of the complexes, water molecules exist in two forms: coordinated water and lattice water (non-coordinated to the metal ion). Coordinated water molecules tend to be lost at higher temperatures (~180 °C), while lattice water molecules are

liberated at lower temperatures (~60-120 °C). The thermo grams reveal that the Cu(II) complexes exhibit remarkable thermal stability up to 250-420 °C, suggesting the presence of solvent or water molecules within the coordination sphere. Decomposition processes in the Cu(II) complexes manifest primarily in two distinct steps. In the first step, a sudden weight loss occurs around 250-320 °C, corresponding to the partial loss of the associated ligand. Subsequently, in the second step, a gradual weight loss appears in the temperature range of 350-600 °C, indicative of the complete decomposition of the organic moiety surrounding the metal ion. [xl, xli]

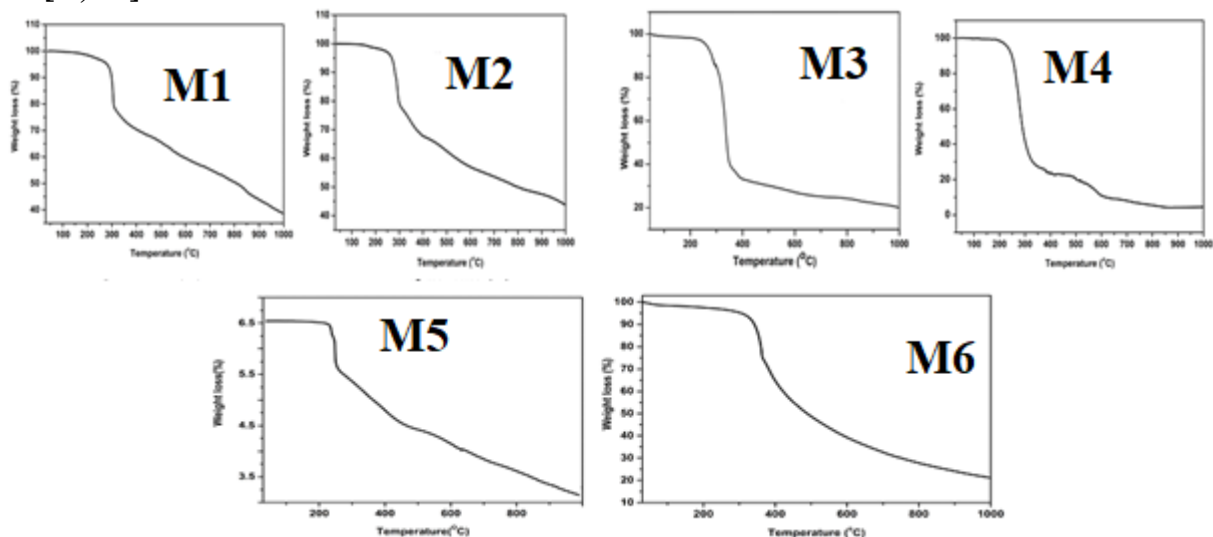


Fig-UL27. TGA spectrum of complex **M1-M6** metal complexes

6.5. Study of electronic absorption spectra

The electronic absorption spectra for both ligands and Cu(II) complexes were meticulously recorded in dimethyl sulfoxide (DMSO) at room temperature, spanning the wavelength range of 200-800 nm. Detailed data is encapsulated in **Table-T4**, while visual representations are depicted in **Fig-UL28**. The electronic spectra of ligands revealed two discernible bands attributed to the $\pi-\pi^*$ transition of the aromatic ring and the $n-\pi^*$ transition of the (HC=N) group [xlii]. Notably, these transitions undergo shifts in metal complexes due to the coordination of ligands with metal ions. Additionally, all copper complexes exhibited distinctive broad d-d transition bands in the visible region. Specifically, the copper complexes displayed two bands corresponding to the $2B_{1g} \rightarrow 2A_{1g}$ and $2B_{1g} \rightarrow 2E_g$ transitions [xliii], indicative of a square planar geometry [xliv]. It's worth noting that square planar complexes are expected to exhibit three possible transitions; however, the observed overlapping of these bands results in either a single or double broad band, as evidenced in the spectra. This characterization contributes to our understanding of the electronic transitions within the Cu(II) complexes and their structural arrangement in a square planar configuration.

Table –T4. Electronic absorption spectra data of Ligands and their **M1-M6** complexes in nm.

Compound	$\pi-\pi^*$ (aromatic)	$n-\pi^*$ (azomethine)	d-d transition
TMMCFP	280	344	-
[Cu(TMMCFP) ₂]	257	381	561
TMMFMOP	277	391	-

[Cu(TMMFMOP) ₂]	259	344	480
TMMFP	263	393	-
[Cu(TMMFP) ₂]	310	392	525
TMMDMOP	280	344	-
[Cu(TMMDMOP) ₂]	256	432	526, 557
TMMBD	391	350	-
[Cu(TMMBD) ₂]	265	414	555
TMMDEP	262	415	-
[Cu(TMMDEP) ₂]	260	336, 428	571

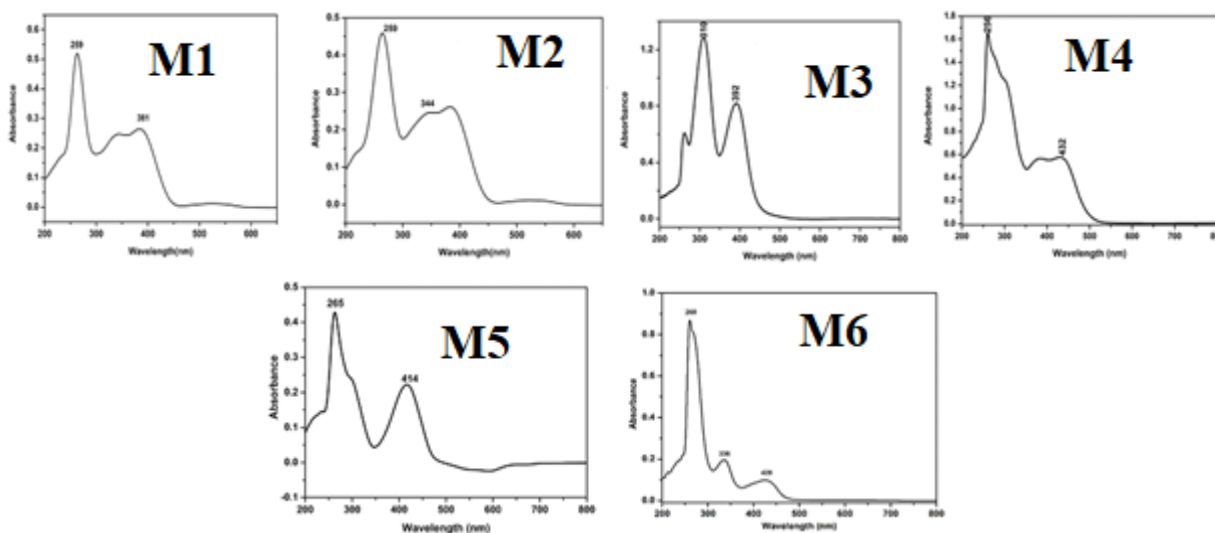


Fig-UL28 Electronic spectrum of complex **M1-M6** metal complexes

6.6. Magnetic susceptibility

Magnetic susceptibility Assessing play a pivotal role in providing valuable information supporting the electronic structure of investigated complexes. In the case of all Cu(II) complexes, denoted as [Cu(TMMCFP)₂] (C1), [Cu(TMMFMOP)₂] (C2), [Cu(TMMFP)₂] (C3), [Cu(TMMDMOP)₂] (C4), [Cu(TMMBD)₂] (C5), and [Cu(TMMDEP)₂] (C6), magnetic susceptibility assessing revealed a paramagnetic character. The observed magnetic susceptibility values, ranging from 1.73 to 1.81 B.M., suggest a square planar geometry with one unpaired electron, consistent with the anticipated electronic configuration of 3d⁹ Cu(II) ions [xliv, xlv]. The assignment of a square planar geometry to all Cu(II) complexes is further supported by electronic spectral data and magnetic moment values, both detailed in **Table-T5**. These magnetic moment values align with the expected characteristics of Cu(II) ions in a square planar coordination environment. Together, magnetic susceptibility measurements and corresponding electronic data contribute to a comprehensive understanding of the electronic and structural properties of the investigated Cu(II) complexes.

Table-T5. Magnetic moment values of metal complexes (**M1-M6**)

Complex	μ_{eff} (BM)
[Cu(TMMCFP) ₂]	1.73

[Cu(TMMFMOP) ₂]	1.76
[Cu(TMMFP) ₂]	1.81
[Cu(TMMDMOP) ₂]	1.78
[Cu(TMMBD) ₂]	1.79
[Cu(TMMDEP) ₂]	1.74

7. Deoxyribonucleic acid interaction studies

7.1. Study of Ultraviolet spectra

Ultraviolet absorption spectroscopy, a fundamental technique, was employed to investigate the coupling interactions of test reagents with DNA [xlvi]. Spectral studies involved mixing fixed concentrations of prepared complexes with varied concentrations of DNA, a widely adopted method for determining binding constants. Changes in the absorption spectrum, specifically hypochromic and hyperchromism, provided valuable insights into the nature of the DNA double helix structure. To discern the binding modes, the complexes were subjected to increasing amounts of DNA, and the resulting spectra were analysed. Hypochromic observed in the absorption spectrum with the addition of DNA suggests an intercalation binding mode, stabilizing the DNA duplex. Conversely, hyperchromism indicates groove binding. The electronic absorption spectra of Cu(II) complexes (M1-M6) were recorded both in the absence and presence of increasing amounts of CT DNA at room temperature. Binding constants (K_b) were calculated by monitoring the π - π^* transition absorption band. The charge transfer peak exhibited hypochromic with a slight shift in λ max, indicative of an intercalative interaction. The calculated K_b values, presented in **Table-T6**, underscore the strong binding affinity of Cu(II) complexes to DNA [xlvi, xlvii]. This comprehensive approach provides valuable insights into the binding mechanisms, highlighting the robust interaction between the studied compounds and DNA. (**Fig-UL29**)

Table-T6. The intrinsic binding constant (K_b) values of binary complexes M1-M6

Complex	K_b (M^{-1})
[Cu(TMMCFFP) ₂] (M1)	2.78×10^5
[Cu(TMMFMOP) ₂] (M2)	4.72×10^5
[Cu(TMMFP) ₂] (M3)	5.23×10^5
[Cu(TMMDMOP) ₂] (M4)	6.52×10^4
[Cu(TMMBD) ₂] (M5)	6.45×10^4
[Cu(TMMDEP) ₂] (M6)	3.03×10^5

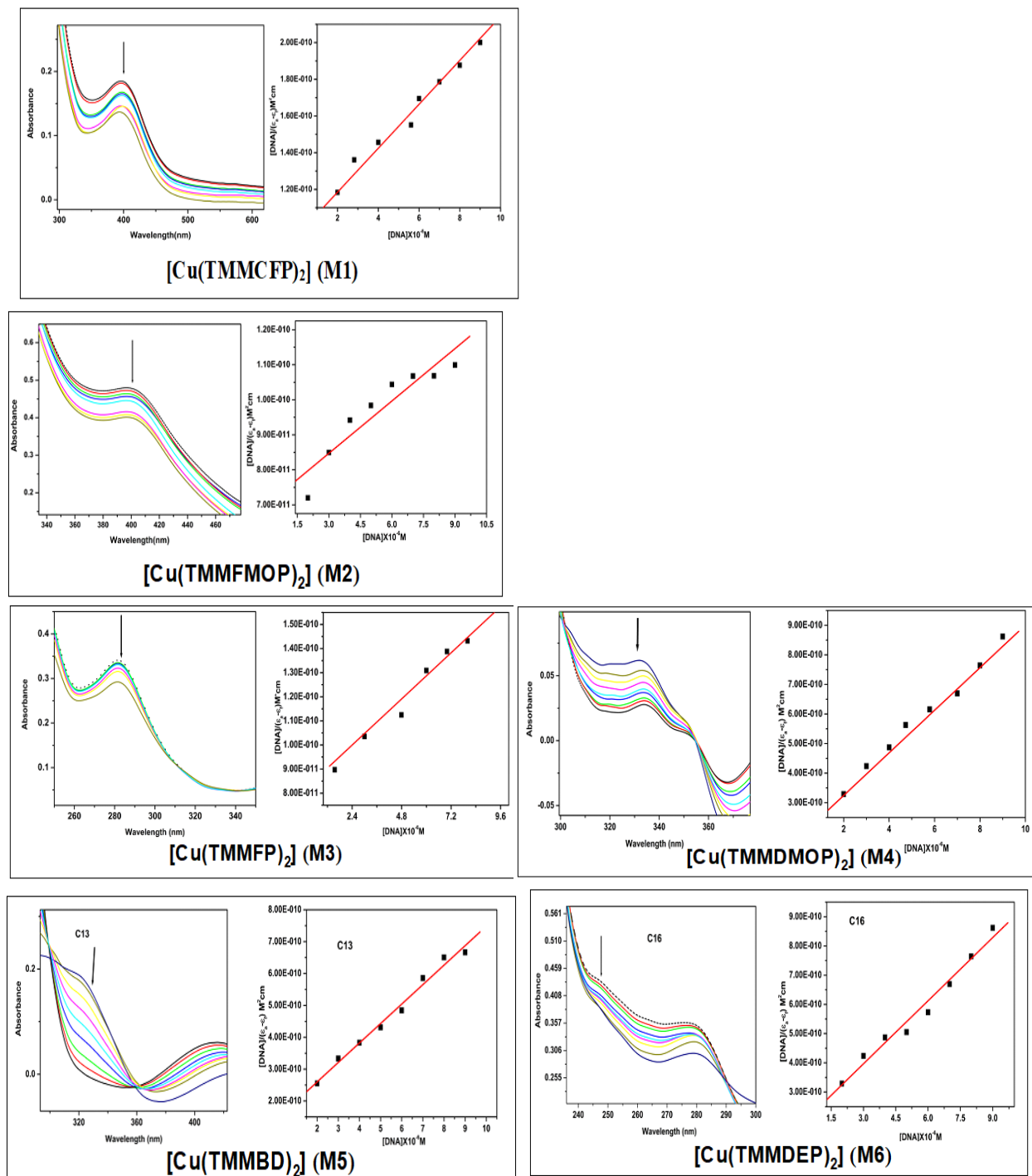


Fig-UL29. UV-Visible absorption spectrum of complex **M1-M6** in the absence (dashed line) and presence (solid lines) of increasing concentrations of CT-DNA. Conditions: [complex] = 10 μM, [CT-DNA] = 0 to 10 μM. Arrow (↓) shows the hypochromism upon increasing DNA concentration. Linear plot for the calculation of the binding constant, K_b .

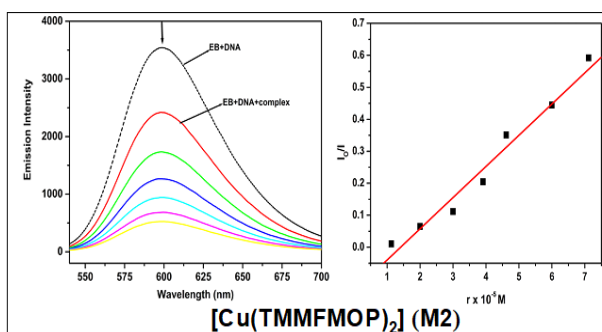
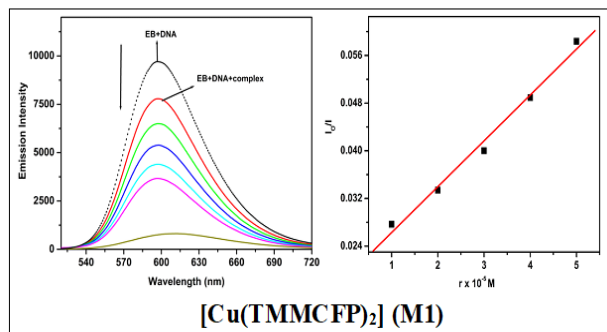
7.2. Fluorescence quenching study

Fluorescence quenching emerges as a valuable approach to explore the reactivity of both chemical and biological systems involving synthesized compounds and DNA. The investigation

of relative binding abilities of complexes with DNA was conducted using the EB-displacement method, where EB, in its free state, exhibited quenched emission in buffer solution. The fluorescence intensity of EB-DNA complex experienced a significant boost upon the addition of CT-DNA, attributable to the strong intercalation between EB and DNA-base pairs. Metal complexes, upon addition, quenched the heightened fluorescence of the EB-DNA system, suggesting their binding to DNA and subsequent replacement of EB. Emission spectra of the EB-DNA system were recorded in the absence and presence of compounds (**M1-M6**), revealing a concentration-dependent decrease in EB-DNA intensity upon addition of metal complexes. The decrease in EB-DNA intensity with increasing concentrations of metal complexes suggests a competitive binding scenario where the complexes vie for binding sites on EB-bound DNA. Fluorescence quenching of EB bound to DNA was observed within the 560-620 nm range, and the degree of quenching was quantified by K_{sv} values calculated from the I_0/I versus r plot. The binding constant K_{sv} values, presented in **Table-T7**, **Fig-UL30** underscore the relative binding affinities of all compounds with CT-DNA, as determined by the classical Stern-Volmer equation. The quenching phenomenon is postulated to arise from the interaction of complexes with DNA through an intercalation mode, with Cu(II) complexes exhibiting stronger binding affinity than Ni(II) and Co(II) complexes. The correlation between the electronic absorption study and the K_{sv} values further supports the conclusion that Cu(II) complexes form stronger bonds with DNA compared to Ni(II) and Co(II) complexes [**I**, **li**].

Table-T7. The Stern-Volmer quenching constant (K_{sv}) values of the Cu(II) complexes.

Complex	K_{sv} (M^{-1})
[Cu(TMMCFP) ₂] (M1)	2.27×10^4
[Cu(TMMFMOP) ₂] (M2)	2.84×10^4
[Cu(TMMFP) ₂] (M3)	2.98×10^4
[Cu(TMMDMOP) ₂] (M4)	1.90×10^4
[Cu(TMMBD) ₂] (M5)	1.20×10^4
[Cu(TMMDEP) ₂] (M6)	2.57×10^4



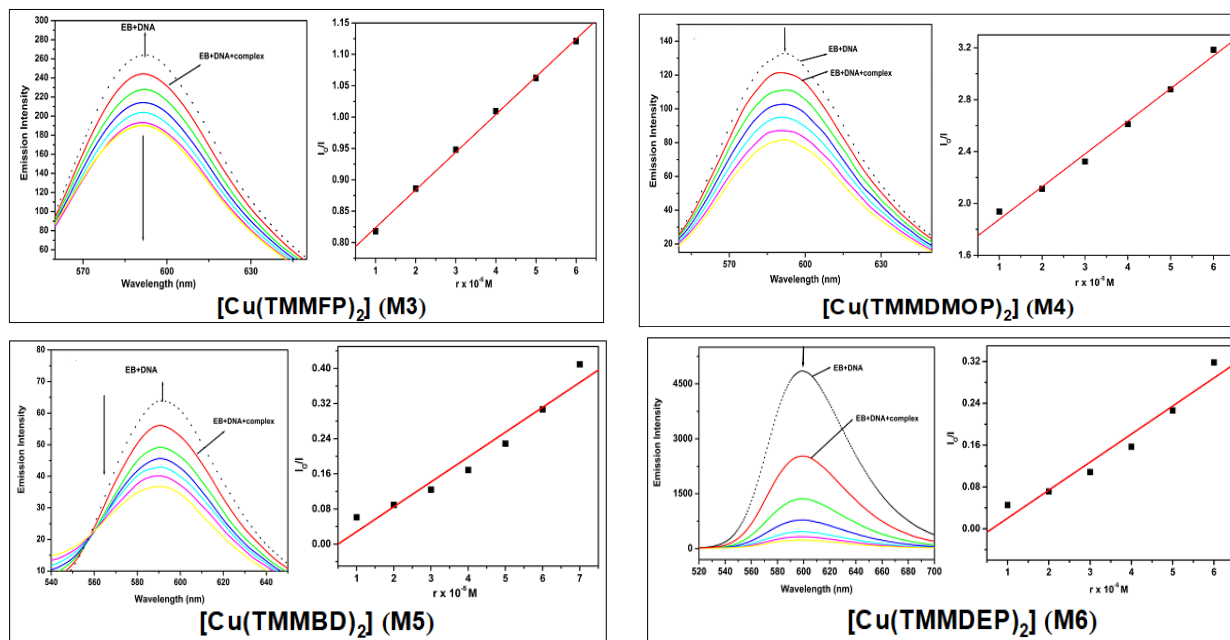


Fig-UL30. The fluorescence quenching spectrum of the EB-DNA system was investigated under varying concentrations of the **M1-M6** complexes, the experimental conditions included [EB] at 12.5 μM , [DNA] at 125 μM , and different concentrations of the complex $[\text{Cu}(\text{TMMFMOP})_2]$ ranging from 0 to 60 μM .

8. Antimicrobial activity

The tabulated antibacterial and antifungal outcomes in Table **Table-T8**, quantified by zone of inhibition diameter (in mm), highlight the remarkable enhancement in antibacterial activity exhibited by the Cu(II) metal complexes, outshining the performance of the **U1-U6** Schiff bases ligands.

Notably, among all the Schiff base ligands, TMMCfP, TMMFMOP, and TMMFP exhibited higher lipophilicity compared to other ligands, contributing to their enhanced uptake in cell membranes. The Cu(II) complexes $[\text{Cu}(\text{TMMCfP})_2]$ (M1), $[\text{Cu}(\text{TMMFMOP})_2]$ (M2), $[\text{Cu}(\text{TMMFP})_2]$ (M3), $[\text{Cu}(\text{TMMDMOP})_2]$ (M4), $[\text{Cu}(\text{TMMBD})_2]$ (M5), and $[\text{Cu}(\text{TMMDEP})_2]$ (M6), demonstrated superior activity, potentially attributed to their enhanced lipophilicity. The heightened activity of Cu(II) complexes can be rationalized by the chelation process, which reduces the polarity of the Cu(II) ion, facilitating its adsorption on the cell wall of microorganisms. This is due to the partial sharing of its positive charge with the orbitals of donor groups in the ligands [lii]. The Cu(II) complexes, particularly $[\text{Cu}(\text{TMMCfP})_2]$, $[\text{Cu}(\text{TMMFMOP})_2]$, and $[\text{Cu}(\text{TMMFP})_2]$, showed greater effectiveness, suggesting a correlation between chelation-induced changes in Cu(II) ion polarity and antimicrobial activity. The variation in complex activity against different microorganisms may stem from differences in the impermeability of microbial cell walls or disparities in ribosomal structures within microbial cells.

Table-T8 provides the zone of inhibition (mm) data for the Schiff bases and their metal complexes (M1-M6), as well as the free metal salt, at a concentration of 500 µg/mL.

Compound	Bacteria (mm)			Fungi (mm)	
	<i>B. amyloliquefaciens</i>	<i>S. aureus</i>	<i>E. coli</i>	<i>M. phaseolina</i>	<i>S. rolfsii</i>
TMMCFP	02±0.2	02±0.3	01±0.3	01±0.2	01±0.4
TMMFMOP	02±0.1	01±0.4	01±0.5	02±0.4	01±0.3
TMMFP	02±0.2	04±0.3	01±0.3	02±0.2	02±0.4
TMMDMOP	01±0.1	01±0.4	02±0.5	02±0.4	02±0.3
TMMBD	01±0.1	01±0.2	01±0.2	02±0.2	01±0.4
TMMDEP	01±0.2	01±0.3	02±0.3	02±0.4	02±0.3
[Cu(TMMCFP) ₂] (M1)	30±0.3	29±0.2	30±0.2	27±0.3	26±0.4
[Cu(TMMFMOP) ₂] (M2)	31±0.4	29±0.2	29±0.1	28±0.3	26±0.1
[Cu(TMMFP) ₂] (M3)	31±0.2	30±0.5	28±0.2	27±0.1	27±0.6
[Cu(TMMDMOP) ₂] (M4)	30±0.4	29±0.2	29±0.1	27±0.3	25±0.1
[Cu(TMMBD) ₂] (M5)	28±0.3	29±0.6	27±0.4	22±0.5	23±0.6
[Cu(TMMDEP) ₂] (M6)	29±0.3	29±0.3	28±0.4	23±0.4	24±0.2
<i>Ampicillin</i>	35±0.2	36±0.2	35±0.2	-	-
<i>Mancozeb</i>	-	-	-	35±0.2	36±0.2

9. Conclusions

A series of free imine bases, namely TMMCFP, TMMFMOP, TMMFP, TMMDMOP, TMMBD, and TMMDEP, derived from 5-(trifluoromethyl)-2-methoxybenzenamine substituted aromatic aldehydes, were successfully synthesized and characterized through various analytical techniques. These include elemental analysis, ¹H & ¹³C-NMR, ESI mass spectrometry, FT-IR, and UV-Visible spectroscopy. Using these ligands, a set of Cu(II) complexes, [Cu(TMMCFP)₂] (M1), [Cu(TMMFMOP)₂] (M2), [Cu(TMMFP)₂] (M3), [Cu(TMMDMOP)₂] (M4), [Cu(TMMBD)₂] (M5), and [Cu(TMMDEP)₂] (M6), were synthesized and thoroughly characterized by elemental analysis, ESI mass spectrometry, FT-IR, UV-Visible spectroscopy, ESR, and TGA. Analytical and spectral studies collectively support a square planar geometry assignment for all the Cu(II) complexes. The interactions between the binary complexes and calf thymus DNA (CT-DNA) were investigated using UV-Vis spectroscopy and fluorescence quenching measurements. These studies revealed that all the binary complexes interacted with CT-DNA through an intercalation mode, indicating a potential for DNA-binding interactions. The antimicrobial activities of both the Schiff bases and their corresponding binary complexes (M1-M6) were studied. The results demonstrated that the complexes exhibited superior inhibitory potentials against various pathogenic microorganisms compared to their Schiff base ligands. Notably, these complexes displayed significant antitumor activity, suggesting their potential in the development of metal-based drugs with promising biological and physiological applications.

10. References

- i H. Abdel-Rahman.; R. M. El-Khatib.; L. A. E. Nassr.; A. M. Abu-Dief.; ,F. E. Lashin.; Design, characterization, teratogenicity testing, antibacterial, antifungal and DNA interaction of few high spin Fe(II) Schiff base amino acid complexes; Spectrochim. Acta A.; 2013, **111**, 266.
- ii L. H. Abdel-Rahman.; R. M. El-Khatib.; L. A. E. Nassr.; A. M. Abu-Dief.; A. A. Seleem; Metal based pharmacologically active agents: Synthesis, structural characterization, molecular modeling, CT-DNA binding studies and *in vitro* antimicrobial screening of iron(II) bromosalicylidene amino acid chelates; Spectrochim. Acta A.; 2014, **117**, 366.
- iii J. P. Costes.; S. Shova.; W. Wernsdorfer.; Tetranuclear [Cu–Ln]₂ single molecule magnets: synthesis, structural and magnetic studies; J. Chem. Soc. Dalton Trans.; 2008, **14**, 1843.
- iv X. G. Ran.; L. Y. Wang.; Y. C. Lin.; J. Hao.; D. R. Cao.; Syntheses, characterization and biological studies of zinc (II), copper (II) and cobalt (II) complexes with Schiff base ligand derived from 2-hydroxy-1-naphthaldehyde and selenomethionine; Appl. Organometal. Chem; 2010, **24**(10), 741-747.
- v Abdel-Rahman, L. H.; El-Khatib.; R. M., Nassr.; L. A., & Abu-Dief. A. M.; Synthesis, physicochemical studies, embryos toxicity and DNA interaction of some new Iron (II) Schiff base amino acid complexes. J. Mol Struct; 2013, **1040**, 9-18.
- vi L. H. Abdel Rahman.; A. M. Abu-Dief.; N. A. Hashem.; A. A. Seleem; Recent advances in synthesis, characterization and biological activity of nano sized Schiff base amino acid M (II) complexes; Int. J. Nano. Chem.; 2015, **1**(2), 79-95.
- vii L. H. Abdel-Rahman.; A. M. Abu-Dief.; S. K. Hamdan.; A. A. Seleem; Nano structure Iron (II) and Copper (II) Schiff base complexes of a NNO-tridentate ligand as new antibiotic agents: spectral, thermal behaviors and DNA binding ability; Int J Nano Chem.; 2015, **1**(2), 65-77.
- viii A. Chakraborty.; P. Kumar.; K. Ghosh.; P. Roy; Evaluation of a Schiff base copper complex compound as potent anticancer molecule with multiple targets of action. Eur. J. Pharmacol.; 2010, **647**(1-3), 1-12.
- ix S.A. Galal.; K.H. Hegab.; A.S. Kassab.; M.L. Rodriguez.; S.M. Kerwin.; A.A. El-Khamry.; H.I. El Diwani; New transition metal ion complexes with benzimidazole-5-carboxylic acid hydrazides with antitumor activity. Eur. J. Med. Chem.; 2009, **44**(4), 1500-1508.
- x J.G.H. Du Preez.; T.I.A. Gerber.; P.J. Fourie.; J. Van Wyk.; The chemistry of rhenium and technetium. Part II. Schiff base complexes with polyfunctional amino acids; J. Coord Chem.; 1984, **13**(2), 173–178.
- xi L.H. Abdel-Rahman.; R.M. El-Khatib.; L.A. Nassr.; A.M. Abu-Dief.; M. Ismael., A.A. Seleem.; Metal based pharmacologically active agents: Synthesis, structural characterization, molecular modeling, CT-DNA binding studies and in vitro antimicrobial screening of iron (II) bromosalicylidene amino acid chelates; M. Bio. Scpet acta A.; 2014, **117**, 366-378.
- xii K. Ghosh.; N. Tyagi.; P. Kumar.; U.P. Singh.; N. Goel.; Stabilization of Mn (II) and Mn (III) in mononuclear complexes derived from tridentate ligands with N2O

- donors: Synthesis, crystal structure, superoxide dismutase activity and DNA interaction studies; *J. Inorg. Biochem*; 2010, **104**(1), 9–18.
- xiii S.M. Abdallah.; G.G. Mohamed.; M.A. Zayed.; M.S. Abou El-Ela.; Spectroscopic study of molecular structures of novel Schiff base derived from o-phthaldehyde and 2-aminophenol and its coordination compounds together with their biological activity.; *Spectrochim. Acta A.*; 2009, **73**(5), 833–840.
- xiv C. Pratiel.; J. Bernadou.; B. Meunier.; DNA and RNA cleavage by metal complexes *Adv.Inorg. Chem*; 1998, **45**, 251–312.
- xv J. Gradinaru.; A. Forni.; V. Druta.; F. Tessore.; S. Zecchin.; S. Quici.; N. Garbalau.; Structural, spectral, electric-field-induced second harmonic, and theoretical study of Ni (II), Cu (II), Zn (II), and VO (II) complexes with [N2O2] unsymmetrical Schiff bases of S-methylisothiosemicarbazide derivatives.; *Inorg. Chem.*; 2007, **46**(3), 884-895.
- xvi B. J. Coe.; N. R. M. Curati.; Metal complexes for molecular electronics and photonics. *Inorg. Chem.*; 2004, **25**(5-6), 147.
- xvii L. H. Abdel-Rahman.; A. M. Abu-Dief.; M. Basha.; A. A. H. Abdel-Mawgoud.; Three novel Ni (II), VO (II) and Cr (III) mononuclear complexes encompassing potentially tridentate imine ligand: Synthesis, structural characterization, DNA interaction, antimicrobial evaluation and anticancer activity.; *Appl. Organometal. Chem*; 2017, **31**(11), 3750.
- xviii S. MojahediJahromi.; M. Montazerzohori.; A. Masoudias.; E.Houshyar.; S. Joohari.; J. M. White.; Sonochemical synthesis and characterization of new seven coordinated zinc, cadmium and mercury nitrate complexes: New precursors for nanostructure metal oxides; *Ultrason. Sonochem*; 2018, **41**, 590-599.
- xix M. Montazerzohori.; S. Farrokhiani.; A. Masoudiasl.; J. M. White.; Crystal structures, Hirshfeld surface analyses and thermal behavior of two new rare tetrahedral terminal zinc(II) azide and thiocyanate Schiff base complexes.; *RSC Adv*; 2016, **6**, 23866.
- xx J. Hine.; C.Y. Yeh.; Equilibrium in formation and conformational isomerization of imines derived from isobutyraldehyde and saturated aliphatic primary amines. *J. Am. Chem. Soc*; 1976, **89**(11), 2669-2676.
- xxi B.S. Kusmariya.; A.P. Mishra.; Co (II), Ni (II), Cu (II) and Zn (II) complexes of tridentate ONO donor Schiff base ligand: synthesis, characterization, thermal, non-isothermal kinetics and DFT calculations; *J. Mol. Str.*; 2017, **1130**, 727-738.
- xxii R.P. Saini.; V. Kumar.; A.K. Gupta.; G.K. Gupta.; Synthesis, characterization, and antibacterial activity of a novel heterocyclic Schiff's base and its metal complexes of first transition series.; *Med. Chem. Res.*; 2014, **23**, 690-698.
- xxiii H. Wang.; X. Zhang.; Y. Zhao.; D. Zhang.; F. Jin.; Y. Fan.; Three Zn (II) complexes with a sexidentate N2O4-donor bis-Schiff base ligand: synthesis, characterization, DFT studies, in vitro antimicrobial evaluation and molecular docking studies; *Inorg. Chim.Acta*; 2017, **466**, 8-15.
- xxiv E. Keskioglu.; A.B. Gunduzalp.; S. Cete.; F. Hamurcu.; B. Erk.; Cr (III), Fe (III) and Co (III) complexes of tetradentate (ONNO) Schiff base ligands: synthesis, characterization, properties and biological activity; *Spectrochim. Acta A.*; 2008, **70**(3), 634–640.
- xxv M. Shabbir.; Z. Akhter.; P.R. Raithby.; L.H. Thomas.; H. Ismail.; F. Arshad.; B.

- Mirza.; S.J. Teat.; K. Mahmood.; Synthesis, characterization and biological properties of novel ON donor bidentate Schiff bases and their copper (II) complexes; *J. Coord. Chem.*; 2017, **70**(14), 2463-2478.
- xxvi Katherine E. Harrison.; Jung F. Kang.; Richard T. Haasch.; S. Michael Kilbey; Surface Structure and Composition of Thiophene-Bearing Monolayers; *Langmuir* 2001, **17**, 21, 6560–6568.
- xxvii Y. Hiromori.; H. Yui.; J. Nishikawa.; H. Nagase.; T. Nakanishi.; Organotin compounds cause structure-dependent induction of progesterone in human choriocarcinoma Jar cells; *J. Steroid Biochem. Mol. Biol*; 2016, **155**, 190-198.
- xxviii P. Kavitha.; M. Rama Chary.; B.V.V.A. Singavarapu.; K. Laxma Reddy.; Synthesis, characterization, biological activity and DNA cleavage studies of tridentate Schiff bases and their Co(II) complexes; *J. Saudi Chem. Soc.*; 2016, **20**(1), 69-80.
- xxix S. Thakurta.; R. J. Butcher.; A. Frontera.; S. Mitra.; Theoretical investigation on molecular structure of a new mononuclear copper (II) thiocyanato complex with tridentate Schiff base ligand.; *J. Coord. Chem.*; 2017, **70**(22), 3715-3726.
- xxx S.S. Jawoor.; S.A. Patil.; S.S. Toragalmath.; Synthesis and characterization of heteroleptic Schiff base transition metal complexes: a study of anticancer, antimicrobial, DNA cleavage and anti-TB activity; *J. Coord. Chem.*; 2018, **71**(2), 271-283.
- xxxi Z.M. Zaki.; S.S. Haggag.; A.A. Soayed.; Studies on some Schiff base complexes of CoII, NiII and CuII derived from salicylaldehyde and o-nitrobenzaldehyde; *Spectrosc. Lett*; 1983, **31**(4), 757–766.
- xxxii S.K. Hoffman.; J. Goslar.; L.S. Szczepaniak.; Weak exchange interaction in cis-Cu (NH₂CH₂COO) ₂·H₂O single crystal: EPR studies; *Phys. Rev.*, 1988, **B37**(13) 7331.
- xxxiii D. Reinen.; C. Friebel.; Cu²⁺ in 5-coordination: a case of a second-order Jahn-Teller effect. II: CuCl₅³⁻ and other CuIII₅ complexes: trigonal bipyramid or square pyramid; *Inorg. Chem.*; 1984, **23**(7), 791-798.
- xxxiv A.H. Maki.; B.R. Mc Garvey.; Electron spin resonance in transition metal chelates. I. Copper (II) bis-acetylacetonate; *J. Chem. Phys.*; 1954, **29**(1), 31-34.
- xxxv R.C. Rosenberg.; A.C. Root; P.K. Bernstein.; H.B. Gray.; Spectral studies of copper (II) carboxypeptidase A and related model complexes; *J. Am. Chem. Soc.*; 1975, **97**(8), 2092-2096.
- xxxvi P. Kamalakannan.; D. Venkappayya; Spectral, Thermal, and Antimicrobial Studies on the Copper (II), Zinc (II), Cadmium (II), and Mercury (II) Chelates of a New Antimetabolite–5-Dimethylaminomethyl-2-Thiouracil.; *Russ. J. Coord. Chem.*; 2002, **28**, 423-433.
- xxxvii P. Sivakumar.; K. S. Parthiban.; M. Vinoba.; S. Renganathan; Optimization of extraction process and kinetics of Sterculia foetida seed oil and its process augmentation for biodiesel production; *Ind. Eng. Chem. Res.*; 2012, **51**(26), 8992-8998.
- xxxviii A.E. S. Ahmed.; T. M. Eldebss; Synthesis, spectral characterization, solution equilibria, in vitro antibacterial and cytotoxic activities of Cu (II), Ni (II), Mn (II), Co (II) and Zn (II) complexes with Schiff base derived from 5-bromosalicylaldehyde and 2-aminomethylthiophene; *Spectrochimica Acta Part A*;

- 2011, **79**(5), 1803-1814.
- xxxix Y. Zhou.; X. Ye.; F. Xin.; X. Xin; Solid state self-assembly synthesis of cobalt (II), nickel (II), copper (II) and zinc (II) complexes with a bis-Schiff base; *Transition Met. Chem.*; 1999, **24**, 118-120.
- xl H. Temel.; H. Alp.; S. Ilhan.; B. Ziyadanogulları.; I. Yilmaz.; *Monatsh.; Spectroscopic and electrochemical studies of transition metal complexes with N, N'-bis (2-aminothiophenol)-1, 7-bis (2-formylphenyl)-1, 4, 7-trioxaheptane and structure effects on extractability of ligand towards some divalent cations; fur. Chem*; 2007, **138**, 1199-1209.
- xli L. H. Abdel-Rahman.; R. M. El-Khatib.; L. A. E Nassr.; A. M. Abu-Dief.; Synthesis, physicochemical studies, embryos toxicity and DNA interaction of some new Iron (II) Schiff base amino acid complexes; *J. Mol. Struct.*; 2013, **1040**, 9-18.
- xlii A. M. Abu-Dief.; L. A. E. Nassr.; Tailoring, physicochemical characterization, antibacterial and DNA binding mode studies of Cu (II) Schiff bases amino acid bioactive agents incorporating 5-bromo-2-hydroxybenzaldehyde; . *Iran. Chem. Soc*; 2015, **12**, 943-955.
- xxliii Laila H. Abdel-Rahman.; Nabawia M. Ismail.; Mohamed Ismael.; Ahmed M. Abu-Dief.; Ebtahal Abdel-Hameed Ahmed; Synthesis, characterization, DFT calculations and biological studies of Mn (II), Fe (II), Co (II) and Cd (II) complexes based on a tetradentate ONNO donor Schiff base ligand; *J. Mole. Struct*; 2017, **1134**, 851-862.
- xliv R.Boča.; M. Breza.; P. Pelikán.; Vibronic interactions in the stereochemistry of metal complexes; *Struct and Bonding*; 1989, **71**, 57.
- xlv W.B. Lewis.; M. Alei.; L.O. Morgan.; Magnetic-Resonance Studies on Copper (II) Complex Ions in Solution. II. Oxygen– 17 NMR and Copper (II) EPR in Aqueous Solutions of Cu (en)(H₂O) 4²⁺ and Cu (en)₂ (H₂O) 2²⁺; *J. Chem. Phys*; 1966, **45**, 4003-4013.
- xlvi Z. Sroubek.; K. Zdanský.; Electron Spin Resonance of Cu²⁺ Ion in CdWO₄, ZnWO₄, and MgWO₄ Single Crystals; *J. Chem. Phys*; 1966, **44**, 3078.
- xlvii R. N. Patel.; N. Singh.; K. K. Shukla.; U. K. Chauhan.; J. Nicols-Gutierrez.; A. Castineiras; Magnetic, spectroscopic, structural and biological properties of mixed-ligand complexes of copper (II) with N, N, N', N'', N''-pentamethyldiethylenetriamine and polypyridine ligands *Inorg. Chim.Acta*; 2004, **357**(9), 2469-2476.
- xlviii D. Kivelson.; R. Neiman.; ESR studies on the bonding in copper complexes; *J. Chem. Phys*; 1961, **35**, 149-155.
- xlix P.F. Rapheal.; E. Manoj.; M.R.P. Kurup.; Copper (II) complexes of N (4)-substituted thiosemicarbazones derived from pyridine-2-carbaldehyde: Crystal structure of a binuclear complex; *Polyhedron*; 2007, **26**(4) 818-828.
- l P. Kamalakannan.; D. Venkappayya.; Spectral, Thermal, and Antimicrobial Studies on the Copper (II), Zinc (II), Cadmium (II), and Mercury (II) Chelates of a New Antimetabolite–5-Dimethylaminomethyl-2-Thiouracil; *Russ. J. Coord. Chem*; 2002, **28**, 423.
- li T. Hirohama.; Y. Kuranuki.; E. Ebina.; T. Sugizaki.; H. Aarii, M. Chikira.; P.T. Selvi.; M. Palaniandavar.; Copper (II) complexes of 1, 10-phenanthroline-derived

- ligands: studies on DNA binding properties and nuclease activity; *J. Inorg. Biochem*; 2005, **99**(5), 1205–1219.
- lii S. Sathiyaraj.; R.J. Butcher.; C. Jayabalakrishnan.; Synthesis, characterization, DNA interaction and in vitro cytotoxicity activities of ruthenium (II) Schiff base complexes; *J. Mol. Struct*; 2012,**1030**, 95-103.

Received on December 27, 2023.